Int J Earth Sci (Geol Rundsch)
DOI 10.1007/s00531-008-0315-2

ORIGINAL PAPER

Estimation of biogenic silica contents in marine sediments using seismic and well log data: Sediment Drift 7, Antarctica

R. C. Neagu · U. Tinivella · V. Volpi · M. Rebesco · A. Camerlenghi

Received: 17 January 2007 / Accepted: 5 April 2008

Abstract Petrophysical properties (wet bulk density, porosity, P-wave velocity) are used to predict biogenic silica contents along a seismic reflection profile that ties two well sites, 1095 and 1096, drilled by Ocean Drilling Program (ODP) Leg 178 on sediment drifts on the Pacific continental margin of the Antarctic Peninsula. The biogenic silica contents along the seismic reflection profile were estimated on the basis of three hypotheses about petrophysical properties distributions in the two boreholes and statistical relationships between biogenic silica and other petrophysical properties, which were established on various sediment layers within the boreholes. Our study demonstrates the possibility to reliably predict the distribution of biogenic silica in the sub-seabed sediments if seismic data processed with amplitude preservation are used and statistical relations are considered. We conclude that the statistical extrapolation of biogenic silica content along seismic reflection profiles tied to borehole data is an efficient tool to quantify the amounts of silica undergoing crystalline transformation, which may have strong implications for submarine slope destabilisation.

R. C. Neagu (✉) · U. Tinivella · V. Volpi · M. Rebesco
Istituto Nazionale di Oceanografia e di Geofisica Sperimentale
42/C, 34010 Sgonico, Trieste, Italy
e-mail: ralukaneagu@gmail.com

A. Camerlenghi
ICREA and GRC Geociències Marines,
Departament d'Estratigrafia, Paleontologia i Geociències Marines, Universitat de Barcelona, C/ Martí i Franquès, s/n,
08028 Barcelona, Spain

R. C. Neagu
3D Lab, School of Earth, Ocean and Planetary Sciences,
Cardiff University, Main Building, Park Place,
Cardiff CF10 3YE, UK

Keywords Antarctic Peninsula · Sediment drifts · Biogenic silica · Opal-A · Opal-CT

Introduction

The presence of large amounts of biogenic silica in marine sediments can affect their physical properties (Bryant et al. 1981). Diagenetic alteration of biogenic opal-A to opal-CT causes a drastic reduction of porosity (about 20 vol% according to Volpi et al. 2003), which contributes to sediment consolidation at depth. The resulting change of acoustic impedance produces a subseafloor bottom-simulating change of reflectivity that is commonly referred to as bottom simulating reflector (BSR) (Lodolo and Camerlenghi 2000). Volpi et al. (2003) have demonstrated that contacts between siliceous microfossils (entire or broken) prevent normal sediment consolidation above the diagenetic front of opal-A/opal-CT transition. The porosity reduction below the diagenetic front may result in overpressuring and decrease in the effective stress. The consequent fluid expulsion to the seafloor affects the stability of the slope as it may lead to gravitational creeping along the weakened surface of the diagenetic front or trigger debris flows (Davies and Clark 2006).

Opal-A is the primary precipitate characteristically amorphous and hydrated with variable amount of water. Opal-CT is a more stable, ordered, crystalline form or phase of silica derived from opal-A after diagenetic reactions. While opal-A is non-crystalline opal, opal-CT consists of clusters of stackings of cristobalite and tridymite over very short length scales. The spheres of opal in opal-CT are themselves made up of tiny microcrystalline

blades of cristobalite and tridymite. Water content may be as high as 10%.

In this study, we attempt a quantitative estimation of biogenic silica content within marine sediments using seismic reflection and physical properties data across the silica diagenesis-induced BSR present in the Pacific margin of the Antarctic Peninsula.

Data set

Well log data

Borehole data are from Ocean Drilling Program (ODP) Leg 178 (Barker and Camerlenghi 1999) that drilled three sites on the upper continental rise northwest of the Antarctic Peninsula. Two of these sites, 1095 and 1096, are located on the sediment Drift 7, following the numbering convention proposed by Rebesco et al. (1997) (Fig. 1). The two sites are crossed by the multichannel seismic reflection profile IT95-135 (Fig. 2).

The composite section drilled at the two sites spans the last 10 Myr. Site 1096, at 3,152 m water depth, recovered a 607 m thick, expanded Early Pliocene–Holocene sedimentary section (Fig. 2). Site 1095, at 3,842 m water depth, recovered a condensed Late Miocene–Holocene sedimentary section. Both sections are assumed to be continuous (Figs. 2, 3).

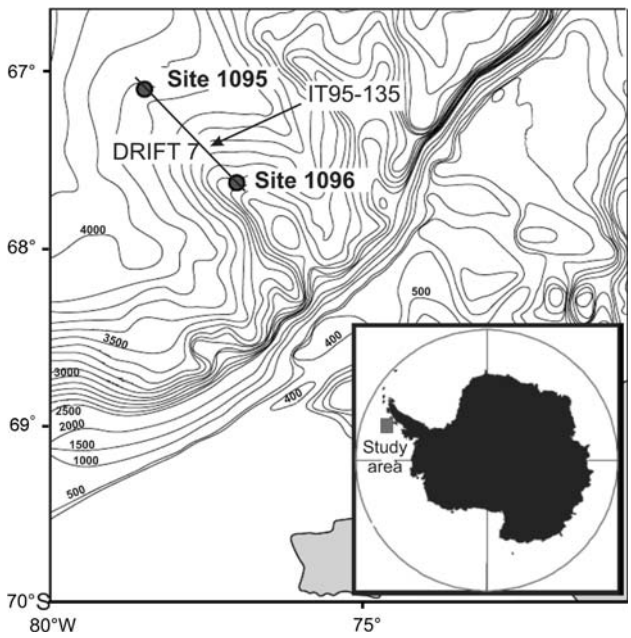

Fig. 1 Location map of the study area. The line crossing ODP sites 1095 and 1096 corresponds to the multichannel seismic reflection profile IT95-135 shown in Fig. 2. Depth contours in metres

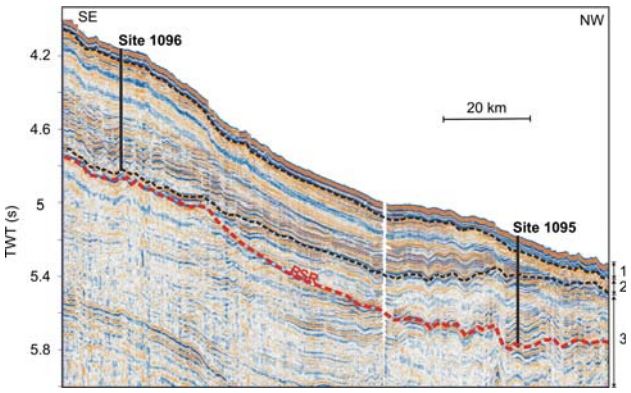

Fig. 2 GI multichannel seismic reflection profile IT95-135. The two *black dashed lines* represent the base of layers 1 and 2, respectively (see main text). The *red dashed line* represents the BSR (bottom-simulating reflector) and also the base of layer 3 (see main text). TWT (s) is the two-way travel time in seconds. Vertical exaggeration is ≈ 1:45. See location in Fig. 1

Because the down-hole logging did not provide reliable data, we used for this study the physical properties data derived from split core measurements from Volpi et al. (2001). Bulk density and porosity measurements were conducted on discrete samples with a spacing of 1.5 m. Velocity data were obtained by using a pair of cylindrical transducers inserted in appropriate parts of the core, and where possible, the data were complemented by Multisensor Track (MST) measurements. The silica data for sites 1095 and 1096 were taken from Hillenbrand and Fütterer (2001) who analyzed core samples using the leaching technique of Müller and Schneider (1993). The vertical profiles of wet bulk density, porosity, velocity and biogenic silica were smoothed using a 5-point adjacent averaging (Fig. 3).

The physical properties at both sites show anomalous consolidation profiles with depth. Porosity minima are reached in between 100 and 200 mbsf at both sites, which are followed by 300 m with no porosity trend with depth at site 1095 and by a slight increasing porosity tendency with depth (~10 vol %) at site 1096 (Volpi et al. 2003) (Fig. 3b). At site 1095, a sharp variation of the physical properties (wet bulk density, porosity, P-wave velocity and biogenic silica content) occurs at ~ 480 mbsf (Fig. 3). In particular, the decrease of porosity corresponds to an increase of wet bulk density and P-wave velocity. In seismic reflection profile this sharp shift results in a positive acoustic impedance contrast responsible for the observed BSR (Fig. 2). Volpi et al. (2003) inferred that intergranular contacts among entire or broken siliceous microfossils above the BSR prevent normal sediment consolidation whereas dissolution of biogenic silica (i.e. dissolution of opal-A) causes sediment consolidation at the silica diagenesis depth, which was only barely crossed at site 1095 (Volpi et al. 2003) (Fig. 2).

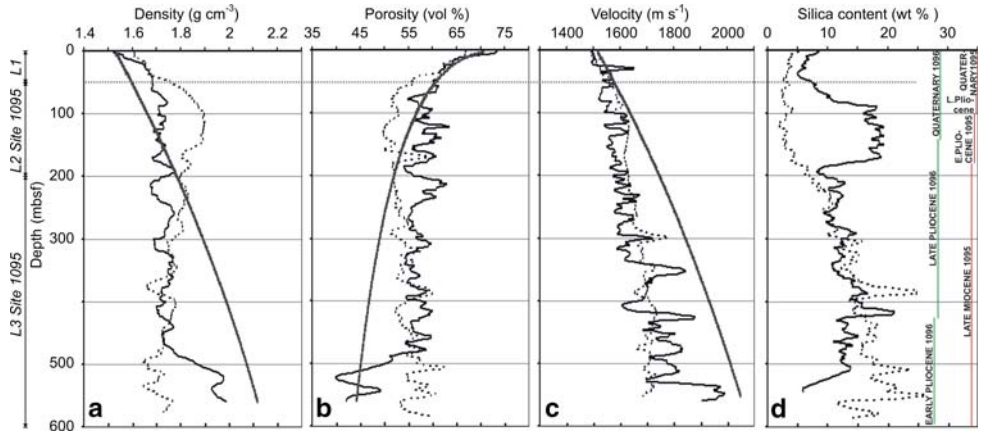

Fig. 3 Plots of (**a**) density; (**b**) porosity; (**c**) P-wave velocity; (**d**) biogenic silica content at ODP sites 1095 and 1096 (see location in Fig. 1). The *dotted lines* correspond to site 1096, and the *thin continuous lines* to site 1095. The *thicker hachured lines* in (**a**–**c**) represent the reference curves. Chronostratigraphy according to Volpi et al. (2003) is presented in *green* for site 1096 and in *red* at site 1095. L1, L2, L3 represent layers 1, 2 and 3 and are explained in "Biogenic silica estimation" of the main text. These layering refers exclusively to site 1095 and was defined from physical properties data

The upper part of the biogenic silica content profiles at both sites (Fig. 3d) is characterised by the lowest values (<10 wt %), which correlate to a significant downhole porosity decrease. Biogenic silica content peaks within the Early Pliocene and the beginning of the Late Pliocene, which corresponds to a depth range of 90–180 mbsf at site 1095 and 300–550 mbsf at site 1096 (Fig. 3d).

Seismic reflection data

In this study, we predict the distribution of physical properties along a multichannel seismic reflection profile named IT95-135 (Figs. 1, 2). The seismic profile was acquired by OGS in 1995 with R/V *OGS-Explora*, using two Generator Injector air guns (Shipboard Scientific Party 1999).

The seismic data were reprocessed using the true amplitude recovery techniques in order to obtain reprocessed images allowing a detailed analysis of the shallow layers. The raw data were filtered using a (30–60 Hz) band-pass filter to suppress high-frequency ambient noise. The velocity analysis was performed every 625 m in order to increase the lateral resolution. A geometric spreading correction was applied to compensate for wavefront divergence. The velocity field was used in normal moveout (NMO) correction of CDP gathers. By checking the amplitude spectrum we verified that the actual signal was not affected by any of the processing steps. Finally, the data were stacked with a 60-fold stack of CDP gathers. No pre- or post-deconvolution and migration techniques were applied to the seismic data set because this would have affected the amplitude.

Methods

Prediction of petrophysical properties using seismic attributes

The prediction of petrophysical properties (P-wave velocity, wet bulk density and porosity) from ODP sites 1095 and 1096 along seismic reflection profile IT95-135 was performed using the EMERGE^{TM} and eLOG^{TM} software packages by Hampson-Russell (Calgary, Alberta, Canada), the latter to perform log data editing, smoothing and log correlation.

A synthetic trace was obtained starting from the density and velocity logs. Averaging four adjacent traces at both sides of the borehole yielded a composite trace. The synthetic trace was aligned to the composite trace near the well location. A time-depth function that maximizes the correlation between the two traces has been computed and used to re-locate and re-calibrate the well logs in time. The input data of the EMERGE^{TM} software are the stacked seismic section and the well log properties. After manually calibrating the well logs to the seismic data with the technique of wavelet extraction and cross-correlation, the wavelet extracted had a length of 180 ms and a taper length of 60 ms.

The EMERGE^{TM} software is able to predict new logs between wells along a tie-seismic reflection profile using seismic attributes as a guide (Hampson et al. 2001). Seismic attributes can be defined as all properties contained in seismics, derived after considering the seismic trace as the actual component of a complex trace (Taner et al. 1979). The basic attributes are instantaneous amplitude, instantaneous phase and instantaneous frequency. Many other attributes can be derived from these ones (Barnes 1998). EMERGE^{TM}

Table 1 Seismic attributes used in Emerge™ (see main text "Methods") to predict the distribution of the physical properties along the seismic reflection profile IT95-135 (see Figs. 1, 2)

Target log prediction	Number of attributes	Attributes	Operator length	Operator lag from center
P-wave velocity	6	Average frequency	3	0
		Filter 15/20–25/30		
		Filter 25/30–35/40		
		Filter 35/40–45/50		
		Integrated absolute amplitude		
		Second derivative		
Density	3	Integrated absolute amplitude	5	0
		Cosine instantaneous phase		
		Instantaneous phase		
Porosity	3	Integrated absolute amplitude	8	0
		Filter 55/60–65/70		
		Raw seismic		

contains a list of 23 attributes, calculated internally from the seismic trace. For more details on seismic attributes see Yilmaz (2001).

The basic algorithm that is used to combine seismic attributes with the target property is linear regression. When applying the so-called single attribute analysis, a linear regression is performed between pairs of seismic attributes and petrophysical properties in order to find a matrix linear relationship:

$$Y = A + BX \tag{1}$$

where X is the matrix in which the elements are the independent variables (target petrophysical properties), Y represents the dependent variables (seismic attributes), and A and B are the two constants that are determined by the regression.

When applying the multiple attribute analysis, the target petrophysical property is modeled as a linear combination of several seismic attributes. Because the linear relationships are often not satisfactory, polynomial relationships with progressively higher order can be used. Different polynomials are computed for an increasing number of seismic attributes. For each computed polynomial, the prediction error is calculated as the root-mean square difference between the actual value and the predicted value of the petrophysical property. A ranking of polynomials is produced according to decreasing errors, and a choice is made of the number of attributes that most significantly predicts a given petrophysical property. The chosen relationship is then used to invert the seismic signal and to predict the spatial distribution of the petrophysical properties along the entire seismic section. Since a linear method produced unreliable results on density distribution prediction along the seismic profile IT95-135, we applied a neural network (EMERGE™ Tutorial; Leiphart and Hart 2001; Dorrington and Link 2004). The number of seismic attributes used for predicting the considered petrophysical properties is presented in Table 1.

Biogenic silica estimation

We propose a simple method for estimating the biogenic silica content of marine sediments. For each borehole we derive a mathematical relationship between the anomalies of sediment petrophysical properties (density and porosity) and the biogenic silica content. The P-wave velocity logs were used for the depth-to-time conversion of the density and porosity logs, since the seismic profile is a time section. The anomaly of the physical property represents the difference between the observed and the reference values. The biogenic silica content is directly correlated with the effective volume it occupies that can be expressed in terms of porosity and density anomalies. The relationships that convert the anomalies of the physical properties into biogenic silica content were extrapolated along the IT95-135 seismic reflection profile (Fig. 2).

For every petrophysical property we calculated a corresponding reference curve (Fig. 3), which represents the expected variation of that property with depth would the sediment be free of biogenic silica.

In order to calculate the reference density (ρ°) we used Hamilton's (1976) relationship for terrigenous sediments (Fig. 3a):

$$\rho^{\circ} = 1.530 + 1.395(z) - 0.617\left(z^2\right), \tag{2}$$

where z is the depth below the seafloor in km.

The reference density increases from 1.5 g cm^{-3} at the sediment surface to 2.1 g cm^{-3} at 600 mbsf (Fig. 3a). The relationships between density and porosity anomalies and the biogenic silica contents were expressed as regressions

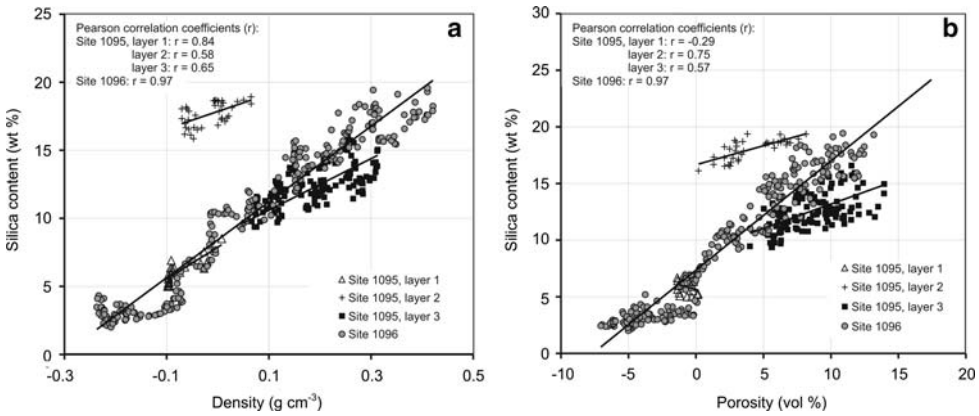

Fig. 4 Cross-plots of biogenic silica content vs (**a**) density and (**b**) porosity anomalies at ODP sites 1095 and 1096 (see location in Figs. 1, 2). While at site 1096 a single regression line fits all points, at site 1095 the points gather in three clusters and, in consequence, three regression lines (one for every layer) were necessary to fit all points

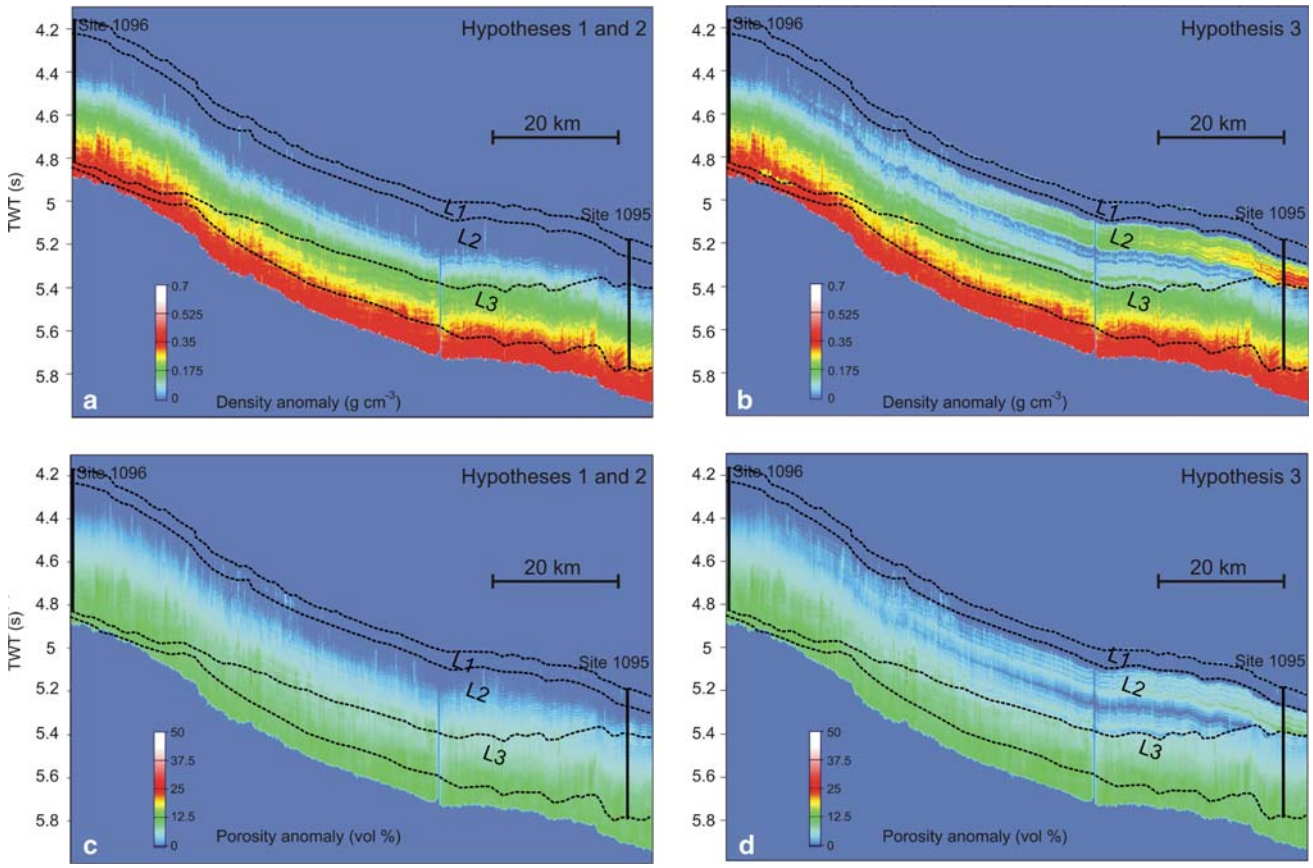

Fig. 5 2D distribution of the (**a** and **b**) density anomaly and (**c** and **d**) porosity anomaly for hypotheses 1, 2 and 3 (see main text "Results") in between sites 1096 and 1095 along seismic reflection profile IT95-135 (see Figs. 1, 2). The *black dashed lines* delimitate layers 1, 2 and 3 (L1, L2 and L3) (see main text "Biogenic silica estimation")

for both drill sites (Fig. 4). The density anomaly reaches a maximum of $\sim$ 0.4 g cm^{-3} at a depth that corresponds to the BSR (Fig. 5a, see also "Results" section).

The reference porosity (ϕ°; Fig. 3b) for both sites was determined using porosity measurements obtained from consolidation tests on samples from the upper, low-biogenic silica section ($\sim$ 5 wt %) at site 1096 (Volpi et al. 2003). The porosity values were then extrapolated for the whole length of the core assuming (1) that the low silica content does not influence the porosity trend with depth and (2) that they could be approximated to that of free-biogenic silica sediments according to:

$$\phi^{\circ} = \frac{74.11 - 11.30}{1 + \sqrt{\frac{z}{335.47}}} + 11.30, \quad (3)$$

where z is the depth below seafloor in m.

The reference porosity decreases from 70 vol % at the sediment surface to $\sim$ 45 vol % at 600 mbsf (Fig. 3b). The

porosity anomaly has a maximum of ~ 13 vol % at the bottom of the sedimentary sequence (Fig. 5c, see also "Results" section).

The reference P-wave velocity (v°) of the sediments was estimated using the relationship proposed by Hamilton (1979) for terrigenous sediments (Fig. 3c) according to:

$$v^\circ = 1.511 + 1.304(z) - 0.741\left(z^2\right) + 0.257\left(z^3\right). \quad (4)$$

The following step in the application of the method is the estimation of the anomaly of the physical property. The linear fits used to describe the relationship between density and porosity anomalies and biogenic silica contents is as follows:

$$c = g + h(x - x^\circ), \quad (5)$$

where c is the biogenic silica content (wt %); g, h are parameters in Table 2; g is Y-axis intercept; h is slope of the linear regression; x° is reference density (g cm^{-3}) or porosity (vol %); x is observed density (g cm^{-3}) or porosity (vol %); x–x° is density anomaly (g cm^{-3}) or porosity anomaly (vol %).

In our case, the observed values are the 2D distributions of density and porosity at the drill sites extrapolated along the seismic profile using EMERGE^{TM}. The anomalies of these parameters are illustrated in Fig. 5 (see also "Results" section).

While at site 1095 three regressions were necessary to describe the relationship of density and porosity with biogenic silica, at site 1096 one single linear regression was enough for the whole sediment column. Consequently, we considered three sediment layers at site 1095 (Figs. 2, 3, 4). They were differentiated according to the correlation between their physical properties with the biogenic silica content. Therefore, the three layers should not be confused with the lithostratigraphic units described by Volpi et al. (2001).

Layer 1, from 0 to 50 mbsf, contains diatom-bearing silty clay and clay of Quaternary age with generally low biogenic silica content. Layer 2 extends from 50 to 200 mbsf and is of Late Miocene to Early Quaternary age. It contains silty clays, silts and fine sands interbedded with massive bioturbated muds of mostly Pliocene age with higher diatom contents. Layer 3, extending from 200 mbsf to the borehole bottom, is of Miocene age and is composed of silty clays, silts and fine sands interbedded with massive bioturbated mud, claystone and siltstone. The biogenic silica content in layer 3 is moderately high.

Results

The distribution of biogenic silica at the two drill sites was estimated starting from the linear regressions presented in the previous section (Fig. 4). Based on these, three hypotheses (H1, H2, H3) have been considered to explain why within layer 2 of site 1095 the increase in the silica content does not correlate to an increase in porosity and a decrease in density (Fig. 3) as it could be expected. In contrast, at site 1096, the silica content increasing trend inversely correlates to a decreasing trend in density and an increasing trend in porosity (Fig. 3). The biogenic silica content was calculated using as input properties the 2D distribution of density and porosity anomalies (Fig. 5). From the cross-plots in Fig. 4, we observe that the cluster of points corresponding to layer 3 at site 1095 is located close to that corresponding to site 1096 and their regression curves have similar parameters (Table 2). For simplification reasons, we used for layer 3 of site 1095 the same linear regression as for site 1096.

H1. We assume that the non-biogenic component of the sediments does not change from one drill site to another. Thus, we applied the same reference curves for density (Fig. 3a) and porosity (Fig. 3b) for both drill sites using equations (2) and (3), respectively. The density and porosity anomalies were converted into biogenic silica contents by applying and extrapolating the relationship determined at site 1096 (Fig. 4) to the whole seismic section. In doing so we further assume that the biogenic silica characteristics (type, state of preservation) do not change from one drill site to another.

Table 2 Values of the parameters utilized in equation (5) within main text to calculate the biogenic silica content, c (wt %)

ODP site	Depth interval (mbsf)	Physical property					
		Density (g cm^{-3})			Porosity (vol %)		
		g	h	x–x°	g	h	x–x°
1096	0–600	8.35	27.90	ρ–ρ°	7.35	0.96	ϕ–ϕ°
1095	Layer 1 (0–50)	7.88	23.55	ρ–ρ°	6.27	0.42	ϕ–ϕ°
	Layer 2 (50–200)	18.04	11.24	ρ–ρ°	16.85	0.26	ϕ–ϕ°
	Layer 3 (200–600)	9.75	14.64	ρ–ρ°	9.24	0.39	ϕ–ϕ°

x–x° is the density (ρ-ρ°) or porosity (ϕ-ϕ°) anomaly; g is the Y-axis intercept; h is slope of the linear regression

H2. As for the first hypothesis, we used the same density and porosity reference curves for both drill sites, assuming the non-biogenic component of the sediments is similar at the two drill sites. We used one relationship for site 1096 and a specific relationship for every of the three layers at site 1095 (Table 2) in order to convert the density and porosity anomalies into biogenic silica contents. In doing so we assumed that characteristics of the biogenic silica change from one drill site to another. The relationships were extrapolated between the two drill sites.

H3. Assuming that the characteristics of the biogenic silica change from one drill site to another, we used three regressions (one per layer) to describe the relationships between silica content and anomalies for density (Fig. 4a) and porosity (Fig. 4b) at site 1095, while at site 1096 we used one single regression (Table 2). The reference curves for both physical properties at site 1096 remain the same as for the previous hypotheses. In contrast to the other two hypotheses, we assume that the non-biogenic components of the sediments change at site 1095 with respect to site 1096. Consequently, we determined two new reference curves for density and porosity at site 1095 (Fig. 6). The reference curves were calculated by rearranging equation (5) and replacing the estimated biogenic silica content with the values measured at the two drill sites. We considered the reference density and porosity as the unknown factors:

$$x^{\circ} = x + \frac{g - c^{*}}{h} \tag{6}$$

where x° is the reference density or porosity for H3; x, g and h as in expression (5); c^{*} is biogenic silica content measured at site 1095 (wt %).

The reference density at site 1095 increases from 1.5 g cm^{-3} at the upper part to 2.1 g cm^{-3} at the bottom of the hole (Fig. 6a).

The reference porosity decreases from 72 vol % at the sediment surface to ~50 vol % until 480 mbsf where it sharply decreases to 37 vol % before reaching the base of the sequence (Fig. 6b).

In between 100 and 180 mbsf, the density anomaly (i.e. the difference between reference and observed densities) has a maximum of 0.35 g cm^{-3} (Figs. 5b, 6a) and the porosity anomaly a maximum of 12 vol % (Figs. 5d, 6b).

The biogenic silica contents obtained from both density and porosity anomalies for the three hypotheses are presented in Fig. 7 and Table 3. The biogenic silica content increases uniformly with depth along the entire seismic profile (Fig. 7a, d) reaching a maximum of 23.3 wt % within layer 3 when using porosity data (Table 3). The maximum difference between silica contents estimated using density and porosity data is 3.6 wt % within layer 1 (Table 3).

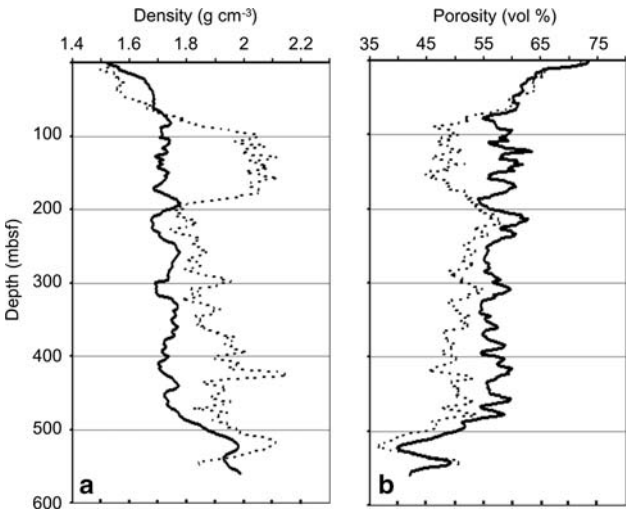

Fig. 6 Reference (**a**) density and (**b**) porosity curves for hypothesis 3 (see main text "Results") at site 1095 (see location in Figs. 1 and 2), and the corresponding observed values (continuous lines)

According to H2**,** biogenic silica contents increase with depth from 13.8 wt % in layer 1 to 21.3 wt % in layer 2, both obtained using density data (Fig. 7b, e). Within layer 3 the estimated silica content reaches a maximum value of 23.3 wt % after porosity data (Fig. 7e). The maximum difference between silica contents estimated using density and porosity data is 4 wt % within layer 1 (Table 3).

Following H3**,** the estimated biogenic silica contents increase with depth. Near site 1095 there is a strong variation of its contents with depth within layer 2 (Fig. 7c, f). Maximum estimated silica contents are 14.6, 21.8 and 23.3 wt % within layers 1, 2 and 3, respectively (Table 3). The maximum difference between silica contents estimated using density and porosity data is of only 2.2 wt % within layer 3 (Table 3).

Discussion and conclusions

Previous attempts similar to the one presented in this paper have been made to statistically predict petrophysical properties along a seismic reflection profile connecting two wells. Coren et al. (2001) utilized Blake Ridge ODP Leg 164 data to predict free gas and gas hydrate contents after converting predicted velocity sections between wells into gas-phase concentration sections. In our case, predicting biogenic silica contents has the advantage of using only simple statistical relationships between petrophysical properties measured on core samples from both wells.

In layer 1, petrophysical properties are more variable (change rapidly with depth) than in the deeper layers, 2 and 3

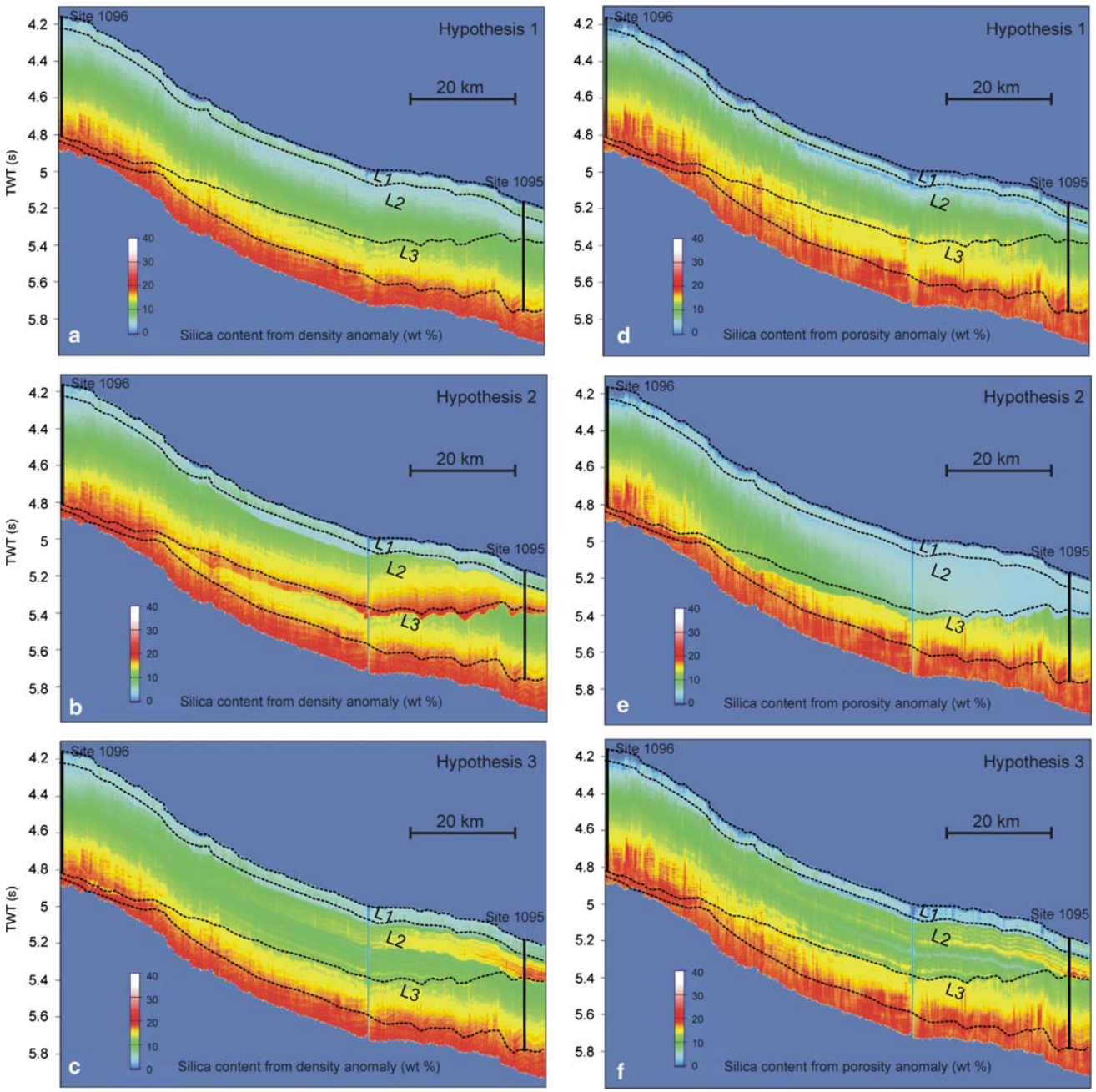

Fig. 7 2D distribution of the estimated biogenic silica content obtained from the (**a**, **b** and **c**) density anomaly and (**d**, **e** and **f**) porosity anomaly for hypotheses 1, 2 and 3 (see main text "Results") in between sites 1096 and 1095 along seismic profile IT95-135 (see Figs. 1 and 2). The *black dashed lines* delimitate layers 1, 2 and 3 (L1, L2 and L3) (see main text section "Biogenic silica estimation")

(Fig. 3). This is because the small amounts of biogenic silica (about 3–8 wt % within layer 1) allow the rapid initial consolidation of the sediments. Conversely, within layers 2 and 3, the biogenic silica is more abundant (Fig. 3d) and intergranular contacts among entire or broken siliceous microfossils prevent normal sediment consolidation.

The estimation of biogenic silica, obtained using density and porosity independently, varies little in general. The maximum difference is 4 wt % within layer 1 after H2 (Table 3).

Contrary to layers 1 and 3 of site 1095, where the biogenic silica content presents similar values to those obtained at site 1096 with no lateral trends between sites, layer 2 displays both lateral and vertical gradients of biogenic silica content. In particular, the silica content increases from site 1095 towards site 1096 and decreases

Table 3 Site 1095 maximum biogenic silica contents (wt %) obtained from density and porosity for the three hypotheses discussed in the main text

Property	Layer	Hypothesis 1	Hypothesis 2	Hypothesis 3
Density	Layer 1	10.2	13.8	14.6
	Layer 2	19.8	21.3	20.0
	Layer 3	21.1	21.1	21.1
Porosity	Layer 1	13.8	9.8	14.6
	Layer 2	21.6	20.6	21.8
	Layer 3	23.3	23.3	23.3

upwards. The upwards decrease was explained by Hillenbrand and Ehrmann (2005) as due to a paleoproductivity change from Early Pliocene conditions with reduced annual sea-ice extent (high productivity) to gradually cooler late Pliocene and Pleistocene conditions with extended sea ice (lower productivity). The statistical extrapolation between the two sites guided by the seismic signal reproduces those trends in biogenic silica contents. The lateral gradient reflects the different sediment accumulation rate between the two sites, and perhaps, an increasing paleoproductivity recorded at the more distal 1095 site due to less sea ice.

Our results show that our third hypothesis H3 is the most reliable. It uses three different relationships for converting physical property anomalies to silica contents and also three different reference curves for density and porosity for the three layers considered. The results obtained with H3 reproduce the lateral and vertical changes expected from sedimentological and paleoceanographical considerations.

The estimated biogenic silica content increases with depth and reaches a maximum of 23.3 wt % at the third layer (Fig. 7; Table 3).

The statistical extrapolation of biogenic silica contents along seismic reflection profiles tied to borehole data potentially is an efficient tool to quantify the amount of silica undergoing crystalline transformation from opal-A to opal-CT and the consequent amounts of pore water released during sediment consolidation at depth. Such quantifications are of prime importance for submarine slope stability assessment as the deep seated transformation of biogenic silica from opal-A to opal-CT is able to trigger slope instability not only at local scale but also at regional scale, as previously shown by Volpi et al. (2003), and Davies and Clark (2006).

Acknowledgments This study has been funded by the EC-FPV Research and Training Network EURODOM (European Deep Ocean Margins: a new training-through-research frontier). Thanks to Hampson-Russell, Calgary, Alberta, Canada for making the software available. Miquel Canals and Claus-Dieter Hillenbrand are gratefully acknowledged for their constructive comments.

References

Barnes AE (1998) The complex seismic trace made simple. Lead Edge 17(4):473

Barker PF, Camerlenghi A (1999) An approach to Antarctic glacial history: the aims of Leg 178. In: Barker PF, Camerlenghi A, Acton GD, et al. (eds) Proceedings of the ocean drilling program, initial report, vol 178, pp 1–44 (CD-ROM)

Bryant WR, Bennett RH, Katerman CE (1981) Shear strength, consolidation, porosity, and permeability of oceanic sediments. In: Emiliani C (ed) The sea, vol 7, Wiley, New York, pp 1555–1616

Coren F, Volpi V, Tinivella U (2001) Gas hydrate physical properties imaging by multi-attribute analysis-Blake Ridge BSR case history. Mar Geol 178:197–210

Davies RJ, Clark IR (2006) Submarine slope failure primed and triggered by silica and its diagenesis. Basin Res 18:339–350

Dorrington KP, Link CA (2004) Genetic-algorithm/neural network approach to seismic attribute selection for well-log prediction. Geophysics 69(1):212–221

Hamilton EL (1976) Variations of density and porosity with depth in deep-sea sediments. J Sediment Petrol 46:280–300

Hamilton EL (1979) Sound velocity gradients in marine sediments. J Acoust Soc Am 65(4):909–922

Hampson DP, Schuelke JS, Quirein JA (2001) Use of multiattribute transforms to predict log properties from seismic data. Geophysics 66(1):220–236

Hillenbrand CD, Ehrmann W (2005) Late Neogene to Quaternary environmental changes in the Antarctic Peninsula region: evidence from drift sediments. Glob Planet Change 45:165–191

Hillenbrand CD, Fütterer DK (2001) Neogene to Quaternary deposition of opal on the continental rise west of the Antarctic Peninsula, ODP Leg 178, sites 1095, 1096, and 1101. In: Proceedings of the ocean drilling program, scientific results, vol 178

Leiphart DJ, Hart BS (2001) Comparison of linear regression and a probabilistic neural network to predict porosity from 3-D seismic attributes in Lower Brushy Canyon channeled sandstones, southeast New Mexico. Geophysics 66(5):1349–1358

Lodolo E, Camerlenghi A (2000) The occurrence of BSRs on the Antarctic margin. In: Max MD (ed) Natural gas hydrate in oceanic and permafrost environments. Kluwer Academic Publ, Dordrecht, pp 199–213

Müller PJ, Schneider R (1993) An automated leaching method for the determination of opal in sediments and particulate matter. Deep-Sea Res 40:425–444

Rebesco M, Larter RD, Barker PF, Camerlenghi A, Vanneste LE (1997) The history of sedimentation on the continental rise west of the Antarctic Peninsula. In: Barker PF, Cooper AK (eds) Geology and seismic stratigraphy of the Antarctic margin, Am. Geophys. Union Antarctic Res Ser, 71(Part 2), pp 29–49

Rebesco M, Pudsey C, Canals M, Camerlenghi A, Barker P, Estrada F, Giorgetti A (2002) Sediment drift and deep-sea channel systems, Antarctic Peninsula Pacific Margin. In: Stow DA, Faugeres JC, Howe J, Pudsey CJ, Viana A (eds) Deep-water contourite systems: modern drifts and ancient series, seismic and sedimentary characteristics. Geological Society, London, Memoirs 22, pp 353–371

Shipboard Scientific Party (1999) Leg 178 Summary. In: Barker PF, Camerlenghi A, Acton GD, et al. Proceedings of ODP, Init. Repts. 178, 1–66. Available from: Ocean Drilling Program, Texas A&M University, College Station, TX 77845-9547, USA

Taner MT, Koehler F, Sheriff RE (1979) Complex seismic trace analysis. Geophysics 44(6):1041–1063

Volpi V, Camerlenghi A, Moerz T , Corubolo P, Rebesco M, Tinivella U (2001) Data report: physical properties relevant to

seismic stratigraphic studies, continental rise sites 1095, 1096, and 1101, ODP Leg 178, Antarctic Peninsula. In: Barker PF, Camerlenghi A, Acton GD, Ramsay ATS (eds) Proceedings of the ocean drilling program, vol 178

Volpi V, Camerlenghi A, Hillenbrand CD, Rebesco M, Ivaldi R (2003) Effects of biogenic silica on sediment compaction and slope stability on the Pacific margin of the Antarctic Peninsula. Basin Res 15:339–363

Yilmaz O (2001) Seismic data processing. In: Stephen Doherty M (ed) Investigations in geophysics, vol 2. Society of Exploration Geophysicists, pp 1–526